Int. J. Heat Mass Transfer. Vol. 10, pp. 623–639. Pergamon Press Ltd. 1967. Printed in Great Britain.

THE EFFECTIVENESS OF THE UNIFORM DENSITY, TWO-DIMENSIONAL WALL JET

W. B. NICOLL* and J. H. WHITELAW
Department of Mechanical Engineering, Imperial College of Science and Technology, London, S.W.7

(*Received* 2 *September* 1966 *and in revised form* 11 *October* 1966)

Abstract—The paper presents new measurements of the effectiveness of a two-dimensional wall jet and a calculation procedure which is shown to closely predict the measured values for a restricted, but practically important, class of injection conditions.

The measurements were performed in the range of slot to free stream mass velocity from 0·467 to 2·26, using helium as a tracer gas and gas chromatographic equipment to detect the relevant concentrations.

The prediction method uses empirical correlations to relate the flow properties at the slot to those downstream of the potential core. Thereafter, an explicit method of solving the boundary-layer equations is employed. The advantages and disadvantages of the method are discussed.

NOMENCLATURE

a, constant (equation 39);
b, constant (equation 39);
C, mass concentration;
$c_f/2$, local drag coefficient ($\tau_S/[\rho u_G^2]$);
F_2, pressure gradient parameter (equation 9);
h, specific enthalpy;
H_{12}, velocity profile shape factor (R_1/R_2);
H_{32}, velocity profile shape factor (R_3/R_2);
l, logarithmic function in drag law (equation 19);
m, mass flow ratio ($\rho_C \bar{u}_C/\rho_G u_G$);
$\dot{m}''_C$, mass flow rate through the slot;
R_1, Reynolds number based upon u_G and δ_1 ($\delta_1 u_G/\nu$);
R_2, Reynolds number based upon u_G and δ_2 ($\delta_2 u_G/\nu$);
R_3, Reynolds number based upon u_G and δ_3 ($\delta_3 u_G/\nu$);
$R_{2,10}$, the value of R_2 at $x/y_C = 10$;
$R_{3,10}$, the value of R_3 at $x/y_C = 10$;
$R_{2,C}$, Reynolds number based on the momentum-deficit of the injected fluid (equation 29);
$R_{2,u}$, Reynolds number based on the momentum-deficit of the mainstream fluid at the slot (equation 30);
R_C, Reynolds number based upon u_C and y_C ($u_C y_C/\nu$);
R_G, Reynolds number based upon u_G and y_G($u_G y_G/\nu$);
$R_{G,10}$, the value of R_G at $x/y_C = 10$;
$R_{\theta,1}$, Reynolds number based on the dimensionless φ profile (equation 14);
R_x, Reynolds number based upon u_G and x (equation 8);
$\bar{s}$, shear work integral (equation 10);
u, velocity in the mainstream direction;
W, width of a free shear layer;
x, distance measured along the wall in the mainstream direction;
y, distance measured normal to the wall;
y_C, slot height;
y_G, velocity boundary-layer thickness;
y_φ, φ boundary-layer thickness.

Greek symbols

δ_1, displacement thickness ($\int_0^{y_G} [1 - u/u_G]\,dy$);
δ_2, momentum-deficit thickness ($\int_0^{y_G} [u/u_G][1 - u/u_G]\,dy$);

* Present address: Department of Mechanical Engineering, The University of Waterloo, Waterloo, Ontario, Canada.

δ_3, kinetic-energy-deficit thickness $(\int_0^{y_G} [u/u_G][1 - u^2/u_G^2]\,dy)$;

Δ, ratio of thickness of conserved property (e.g. enthalpy or concentration) to momentum boundary layers (y_φ/y_G);

ζ, shape factor (equation 20);

ξ, dimensionless distance from the wall (y/y_G);

ρ, fluid density;

τ, total (laminar plus turbulent) shear stress;

τ_S, value of τ at the wall $(y = 0)$;

ν, kinematic viscosity of the fluid;

φ, a conserved property;

η_I, impervious wall effectiveness (equation 2);

η_T, adiabatic wall effectiveness (equation 1);

η, effectiveness based upon the general conserved property φ (equation 15).

Subscripts

C, pertaining to the flow through the slot;

G, pertaining to the mainstream $(y > y_G)$;

S, pertaining to the wall $(y = 0)$.

1. INTRODUCTION

THE INJECTION of a secondary fluid stream into a boundary layer to provide a film of cooler fluid adjacent to the surface is termed "film cooling"; it finds application in rocket and jet engines. The injection of a warmer secondary fluid, which by analogy might be termed "film heating", is also of technical importance, for instance, in the prevention of icing on aircraft wings. A measure of the efficacy of either film cooling or film heating is the effectiveness, η_T, defined by

$$\eta_T \equiv \frac{h_S - h_G}{h_C - h_G} \tag{1}$$

where h is the specific enthalpy; and where the subscripts S, G and C refer to the surface, the mainstream, and the injected fluid respectively. In the particular case where the surface is impervious to the flow of heat, it is common to refer to the "adiabatic-wall-effectiveness"; the present work is concerned with this case only.

A critical review of previous experimental studies of adiabatic wall effectiveness [1–12] has been presented by Whitelaw [13]. He shows that, for identical mean injection to mainstream mass velocity ratios, m, and for identical injection Reynolds numbers, the measurements of various investigators differ by large amounts, sometimes by percentages of hundreds. There are many possible reasons for these discrepancies, such as non-uniform density, non-adiabatic walls, lack of two-dimensionality, the various turbulence levels, the geometry of the injection region, the thickness of the upstream boundary layer, etc. One of the objectives of the present work is partially to illuminate this problem.

The measurements reported in this paper represent the first stage of a comprehensive investigation of the effectiveness of film cooling. They are confined to simple two-dimensional injection slots and represent measurements of the *impervious wall effectiveness* rather than the *adiabatic wall effectiveness*: i.e. in place of the more usual method of injecting a gas of enthalpy different from the main stream and measuring the enthalpy at the wall at downstream locations, a tracer of helium was injected into the second fluid and the wall concentration of this tracer was measured at downstream locations. The present technique allows the simultaneous attainment of an impervious wall, sensitive measurement and uniform density. The impervious wall effectiveness is defined by

$$\eta_I = \frac{C_S - C_G}{C_C - C_G} \tag{2}$$

where C is the mass concentration of the tracer gas, and where the subscripts have the same significance as in equation (1). The impervious wall effectiveness, η_I, and the adiabatic wall effectiveness, η_T, are governed by identical

equations and may be said to be equivalent if the total (laminar plus turbulent) Lewis number is unity. Comparison of prediction and experiment, using the present prediction method, support the hypothesis of unity Lewis number.

Many previous attempts to predict the effectiveness of film cooling, such as those contained in references [1–12], have been of an empirical nature and have offered little hope of extension to flow situations which involve any extension of the two-dimensional, constant property, zero pressure-gradient configuration with which most measurements have nominally been made. Further, two different correlations are normally required to account for flow with the free-stream velocity greater than the slot velocity and for flows with the slot velocity greater than that of the free stream: both cases are of interest since values of the ratio of slot to free-stream velocity from 0·2 to 1·5 are found in practice. The correlation equation suggested by Spalding *et al.* [14, 15] was devised to overcome this drawback but the equation deviates considerably from many measurements and offers little hope of extension to more complex flows.

The methods of solving the boundary-layer equations presented by Spalding [16] and Patankar and Spalding [17] are valid for values of the mass flow parameter, m, greater or less than unity: they may be used to predict the adiabatic wall effectiveness. The relative merits of these approaches and of the present approach are discussed in Section 5.

Reference [18] contains a more detailed description of the solution of the hydrodynamic equations, than is given in this paper. The present paper represents an extension of the work contained in reference [18] to include the solution of the energy equation for the adiabatic wall case.

2. PRESENT MEASUREMENTS

2.1 *Description of apparatus and experimental method*

The basic requirements of the present experimental investigation were a two-dimensional, low-turbulence free stream, a two-dimensional secondary stream of density equal to that of the free stream but with a detectable tracer gas, zero pressure gradient and an impervious wall. The free stream was provided by a blower and a contraction which supplied air in the 18 × 12-in working section at a velocity of approximately 70 ft/s with a turbulence of 0·5 per cent. Secondary air, which included a tracer of helium, was injected along the base plate of the wind tunnel working section by means of a secondary blower and a slot as shown in Fig. 1. A detailed drawing of the slot is provided in Fig. 2.

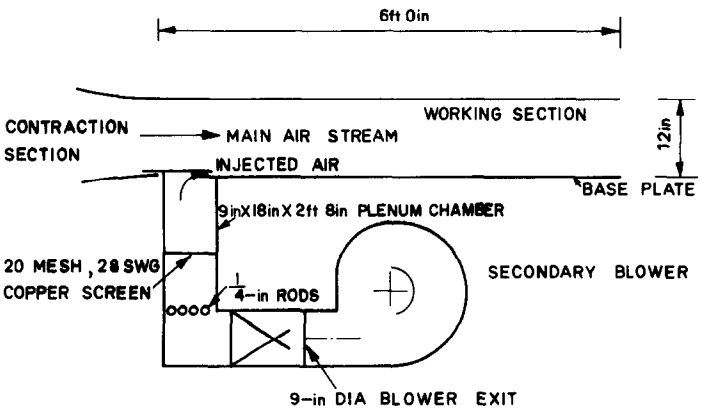

FIG. 1. General arrangement of working section and secondary air system.

Only measurements of velocities and of wall concentration were required in the present investigation. Velocity profiles were measured in the exit plane of the slot and at a distance of ten slot heights downstream. The former was integrated to provide the mass flow through the slot and the latter was related to the former as shall be seen later. The velocities were computed from measured values of total head pressure using a flattened total head probe of internal dimensions 0·053 × 0·0036 in and from measured static pressures using static pressure taps of 0·020-in dia. in the base plate of the tunnel working section.

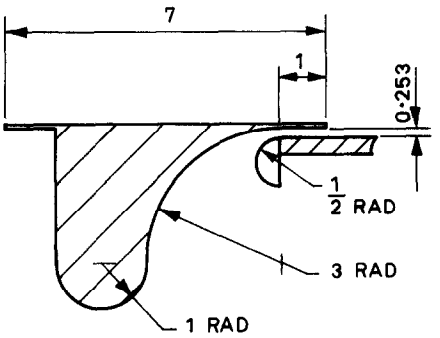

FIG. 2. Slot configuration. (Dimensions in inches.)

The impervious wall effectiveness is defined by equation (2) and since, for the present measurements C_G is negligible,

$$\eta_I = \frac{C_S}{C_C}. \tag{3}$$

Thus it is only necessary to measure the concentration of the tracer gas, i.e. helium, in the exit plane of the slot and at downstream locations. This was accomplished by sucking samples of the air plus helium mixture through the tunnel base plate at selected locations downstream and measuring the helium concentration with the aid of a gas chromatograph. The concentration of helium in air of the secondary stream at exit from the slot was in the region of 1 per cent by volume and the sampling method was arranged to economise on the quantity of helium expended and consequently on the running time of each test.

Several features of the apparatus described above, and of the procedures employed, require detailed explanation; these are given below.

2.1.1 *Sampling method.* Having selected helium as the tracer gas it was not economically possible to have it flowing for a lengthy period of time. Consequently continuous flow measurements were ruled out and a method had to be found of obtaining samples in a short time (say 3 or 4 min) and measuring their concentration after the tracer gas had been shut off. The apparatus designed for this purpose is shown in Fig. 3. It consists of a series of 15 bottles of 20-ml capacity with a glass valve at the bottom end. The bottom stem of each bottle is sealed into a large vessel and projects downwards into a pool of high vacuum oil. The upper stem is connected through a piece of thick wall rubber tubing to an additional valve and thence, by means of small

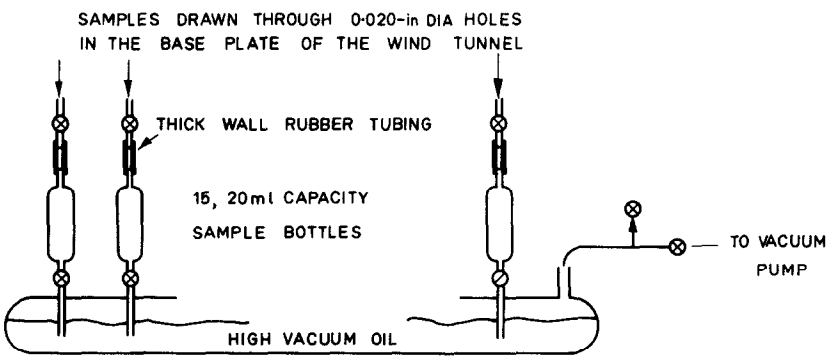

FIG. 3. Sampling system.

bore pvc tubing, to the selected 0·020-in dia. holes in the base plate of the wind tunnel.

To measure the effectiveness of a particular jet configuration, the two fans were switched on and the velocities adjusted to the selected values. The two valves on each sampling bottle were opened and air pressure applied through the T-piece provided until the oil level in each bottle was close to the upper valve. The upper valves were then closed, the pressure connection closed off and the vacuum connection opened. The vacuum pump was turned on. Helium was then added to the secondary air flow at inlet to the fan, the flow rate of helium being measured by a Rotameter.

The air and helium were allowed to flow for about 15 s and then the upper valves on all bottles were opened and the oil sucked into the large glass vessel flushing each bottle. The air–helium mixture was allowed to flow through each bottle for approximately 2 min and then both valves on each bottle were closed and the helium and vacuum pump turned off. The mixture in each bottle was then ready for sampling at leisure. For all of the measurements recorded in this paper, the sampling procedure began shortly after the helium flow had been shut down. Sampling was effected with the aid of a 1-ml gas-tight syringe, samples being obtained by piercing the thick wall rubber tubing with the needle of the syringe. Samples obtained in this way were immediately injected into the chromatograph.

It was necessary to ensure that the concentration of any particular sample was not affected by the rate of sampling. Consequently, various sampling rates were investigated and the values of impervious wall effectiveness reported in this paper were all obtained using sampling rates within a range which experiment showed to be free from sampling rate effects.

2.1.2 *Detection method.* The gas chromatograph used to measure the helium concentration of each sample employed a 2-m long column, packed with Linde type Molecular Sieve, to separate the permanent gases and a thermal conductivity cell to measure their concentration. Nitrogen was used as carrier gas and consequently helium and oxygen provided the only two significant peaks. The column temperature was arranged so that both the helium and oxygen passed through the column in less than 3 min. The thermal conductivity cell was calibrated for helium detection over the working range of concentration.

The use of a hypodermic syringe for gas injection resulted in a slight uncertainty in the amount of gas injected. However, the oxygen peak provided a sufficiently sensitive check on the total volume of gas injected and consequently, the ratio of helium to oxygen peak heights was used for calibration and for measurements of effectiveness. The value of the impervious wall concentration was, thus, calculated from

$$\eta_I = \frac{(\text{helium peak height/oxygen peak height})\, x = x_1}{(\text{helium peak height/oxygen peak height})\, x = 0}.$$

2.1.3 *Two-dimensionality of flow.* The two-dimensionality of the air flow was checked with the aid of the total head probe at various locations in the tunnel. No significant deviations from two-dimensional flow were detected in the initial 4 ft 6 in of the working section.

The two-dimensionality of the tracer gas is also of importance and this was checked at various x-locations, by measuring the wall concentration on the centre line of the tunnel base plate and at points 3 in on each side of this centre line. In some cases, discrepancies in the local values of effectiveness were detected but subsequent measurements with different transverse effectiveness profiles, indicated that the magnitude of the non-two-dimensionality was not significant.

2.2 *Results**

The values of the impervious wall effectiveness obtained using the methods described above, are shown on Fig. 4. This figure depicts the

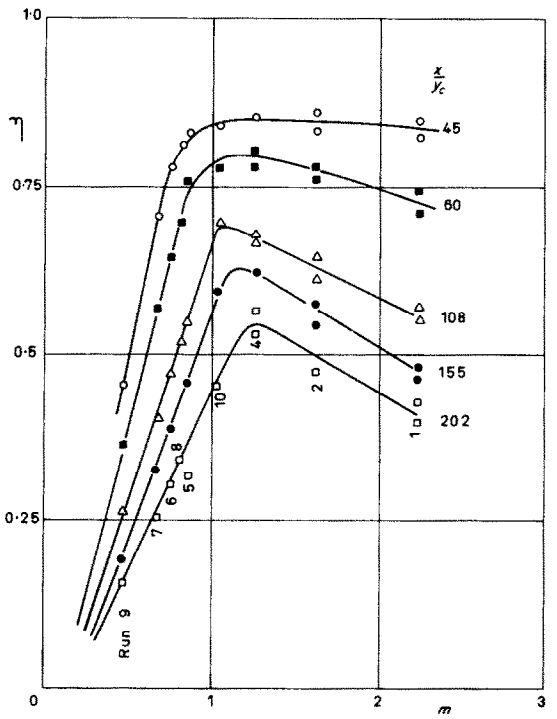

FIG. 4. The impervious wall effectiveness at various downstream locations.

impervious wall effectiveness against the parameter m, i.e. the ratio of slot to free-stream mass-flow velocity. These axes were chosen because they provide a relatively clear view of the experimental reproducibility. The data were obtained using three different slot heights which were nominally the same: these are shown in Fig. 5. For all of these measurements, the pressure gradient measured along the tunnel was negligible.

It may be seen from Fig. 4 that some of the effectiveness measurements were duplicated. Initially, effectiveness measurements were made for runs 1 and 2 using the slot shown in Fig. 5(a) —several sets of measurements were made and these were averaged to yield one of the points shown for runs 1 and 2 on each line of constant x/y_C. Similarly, one of the points attributed to each of runs 4 and 5 were obtained using the slot shown in Fig. 5(b). All other points were obtained using the slot shown in Fig. 5(c). This serves to indicate that the results are reproducible to, at worst, 7 per cent of the local value of effectiveness, i.e. less than 3 per cent of the

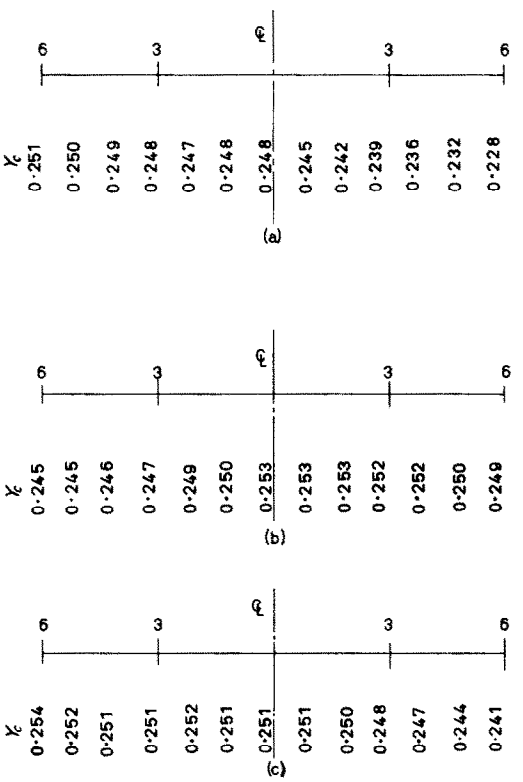

FIG. 5. Variation of slot height over centre 12 in. (Dimensions in inches.)

maximum value, and that this discrepancy may be due in part to the departures from two-dimensional flow. (These results are also shown on more conventional coordinates in Fig. 10

* These results are obtainable in tabulated form in reference [19] which also gives a more detailed description of the apparatus and of the experimental procedure.

where the measurements are compared with the values which are predicted using the method described in Section 3.)

3. METHOD OF PREDICTION

3.1 *Integral equations*

Downstream of the immediate vicinity of the slot, the experimental velocity profiles have been shown by Spalding [16] and by Escudier and Nicoll [20] to be adequately described by two parameters. In the present work the Reynolds numbers R_2 and R_3 are used: these are defined as

$$R_2 \equiv \frac{\delta_2 u_G}{\nu} \tag{4}$$

and

$$R_3 \equiv \frac{\delta_3 u_G}{\nu} \tag{5}$$

where δ_2 and δ_3 are the momentum and kinetic-energy thicknesses respectively, u_G is the main stream velocity and ν is the kinematic viscosity of the fluid.

With the usual boundary-layer assumptions, the integral equations describing the development of R_2 and R_3 may be written as

$$\frac{dR_2}{dR_x} + (1 + H_{12}) F_2 = c_f/2 \tag{6}$$

and

$$\frac{dR_3}{dR_x} + 2H_{32} F_2 = 2\bar{s}. \tag{7}$$

In these equations, R_x is the Reynolds number based on u_G and x, the distance measured along the wall in the main stream direction; it is defined as

$$R_x \equiv \int_0^x (u_G/\nu)\, dx. \tag{8}$$

F_2 is the pressure-gradient parameter defined by

$$F_2 \equiv R_2\, d(\ln u_G)/dR_x. \tag{9}$$

The shape factors H_{12} and H_{32} are defined respectively as the ratios δ_1/δ_2 and δ_3/δ_2, where δ_1 is the displacement thickness; $c_f/2$ is the local drag coefficient and $\bar{s}$ is the shear work integral which may be defined by

$$\bar{s} \equiv \int_0^{y_G} [\tau/\rho u_G^3]\, (\partial u/\partial y)\, dy \tag{10}$$

where τ is the total shear stress and y_G the boundary-layer thickness.

Equations (6) and (7) represent two of the three integral equations which have to be solved. The third equation is the equation of conservation of a property which may (in the present context) be enthalpy or concentration. This equation may be written as

$$\frac{d}{dR_x}\left\{ \int_0^\infty \rho u(\varphi - \varphi_G)\, dy \right\} = 0 \tag{11}$$

where φ represents the conserved property. Equation (11) may be rewritten in the form

$$\frac{d}{dR_x}\left\{ \frac{u_G (\varphi_S - \varphi_G)}{\nu (\varphi_C - \varphi_G)} \int_0^\infty \frac{u}{u_G}\left(\frac{\varphi - \varphi_G}{\varphi_S - \varphi_G} \right) dy \right\} = 0 \tag{12}$$

or

$$\frac{d}{dR_x}(\eta R_{\theta,1}) = 0 \tag{13}$$

where

$$R_{\theta,1} \equiv \frac{u_G}{\nu} \int_0^\infty \frac{u}{u_G}\left(\frac{\varphi - \varphi_G}{\varphi_S - \varphi_G} \right) dy \tag{14}$$

and

$$\eta = \frac{\varphi_S - \varphi_G}{\varphi_C - \varphi_G}. \tag{15}$$

Thus it is necessary to solve equations (6), (7) and (13) in order to determine the value of effectiveness. The next sub-section presents the auxiliary equations required for the solution of these equations, and sub-section 3.3 the initial correlations which relate the initial values of R_2 and R_3 and η to the flow properties at the slot.

3.2 *Auxiliary equations*

In order to solve equations (6) and (7), relationships are required between the quantities H_{12}, $c_f/2$ and $\bar{s}$ and the dependent variables R_2 and R_3. The three relationships used in this paper are

$$\text{(i)}\quad H_{32} \equiv \frac{R_3}{R_2} = \begin{cases} 1{\cdot}421 - 0{\cdot}0971/H_{12} + 0{\cdot}775/H_{12}^2; & 2{\cdot}8 > H_{12} \geqslant 1{\cdot}25 \\ 2{\cdot}674 - 0{\cdot}66H_{12}; & 1{\cdot}25 \geqslant H_{12} \geqslant 0{\cdot}85 \\ 0{\cdot}82 + 1{\cdot}10/H_{12}; & 0{\cdot}85 \geqslant H_{12} > 0{\cdot}06 \end{cases} \tag{16}$$

$$\text{(ii)}\quad c_f/2 = \frac{0{\cdot}243\zeta^2 + 0{\cdot}03759\zeta - 0{\cdot}00106 + 0{\cdot}0914\zeta^2/(1 + 65/\zeta)}{l^2} \tag{17}$$

$$\text{(iii)}\quad \bar{s} = \tfrac{1}{3}(1 + 2\zeta)\, c_f/2 + \begin{cases} 0{\cdot}0056(1-\zeta)^{2{\cdot}715}; & \zeta \leqslant 1 \\ 0{\cdot}01(\zeta - 1)^3 & \zeta \geqslant 1. \end{cases} \tag{18}$$

In these equations ζ and l are defined as

$$l \equiv \ln\left[\frac{3{\cdot}389\, R_2\zeta}{(1-\zeta)(1+2\zeta)}\right] \tag{19}$$

$$\zeta \equiv \tfrac{2}{3}H_{32} - 1 + \sqrt{[\tfrac{2}{3}H_{32}(\tfrac{2}{3}H_{32} - 1)]}. \tag{20}$$

These auxiliary equations, and their origins, are described in more detail in reference [18] and are repeated here for completeness.

A further auxiliary equation is required to relate $R_{\theta,1}$ to hydrodynamic quantities. This relationship could be obtained in the same manner as the auxiliary equations, equations (16–18) (i.e. from experimental data) if suitable data were available. However, this data is not available and consequently profile assumptions must be made and the required relationship derived from the assumed profiles. Two profile assumptions are required: one for the velocity profile and one for the profile of the conserved property φ. Both profiles are here assumed to be straight lines, i.e. it is assumed that

$$u/u_G = A + (1 - A)y/y_G \tag{21}$$

and

$$\frac{\varphi - \varphi_G}{\varphi_S - \varphi_G} = (1 - y/y_\varphi) \tag{22}$$

where y_G and y_φ are the thickness of the velocity and conserved-property boundary layer respectively.

At first sight the assumptions contained in equations (21) and (22) appear to be crude and grossly in error. In fact the linear velocity profile has been shown by Escudier *et al.* [21] to be remarkably satisfactory for predicting *integral* quantities and the use of a linear φ profile is substantiated by the measurements of Seban and Back [22] which show that the temperature profile downstream of a film cooling slot is very close to linear for values of the non-dimensional distance, x/y_C, greater than 20.*

Equation (21) may be inserted into the definitions of R_2 and R_3 and an expression for H_{32} can subsequently be derived. The performance of this exercise demonstrates that the constant A in equation (21) is identical to the parameter ζ of equation (20). Thus the required auxiliary relationship can be written as

* This suggests immediately one limitation of the present assumptions, i.e. that the predicted values of effectiveness very close to the slot are likely to be in error. This will later be shown to be the case.

$$R_{\theta,1} = \frac{u_G}{\nu} y_G \int_0^\infty [\{\zeta + (1-\zeta)\, y/y_G\} \times \{(1 - y/y_\varphi)\}]\, \mathrm{d}y/y_G \qquad (23)$$

or

$$R_{\theta,1} = R_G \int_0^\infty [\{\zeta + (1-\zeta)\,\xi\}\{1 - (\xi/\Delta)\}]\, \mathrm{d}\xi. \qquad (24)$$

where

$$\xi = y/y_G \quad \text{and} \quad \Delta = y_\varphi/y_G.$$

Equation (24) may be integrated to yield (for $\Delta > 1$)

$$R_{\theta,1} = \frac{R_G}{6}\left[(\zeta - 1)\left(3 - \frac{1}{\Delta}\right) + 3\Delta\right]. \qquad (25)$$

From the definitions of R_G and R_2 and from equation (21), it may readily be shown that

$$R_G = \frac{6R_2}{(1-\zeta)(1+2\zeta)} \qquad (26)$$

so that the required auxiliary equation is

$$R_{\theta,1} = \frac{R_2}{(1-\zeta)(1+2\zeta)} \times \left[(\zeta - 1)\left(3 - \frac{1}{\Delta}\right) + 3\Delta\right]. \qquad (27)$$

The value of the dimensionless thickness, Δ, must be chosen before equation (27) can be utilized. Examination of the effectiveness measurements reported in the present paper suggested a value for Δ of 1·25 and this value was used for the predictions reported in Section 4. It should be noted that the selection of a constant value for Δ, implies that the predictions for effectiveness are likely to be in error for flow configurations which involve a thick boundary layer on the upper lip of the slot.

3.3 *Initial conditions*

The two hydrodynamic equations, equations (6) and (7), together with the auxiliary equations (16–18) may be solved to yield values of R_2 and R_3 as functions of the independent variable R_x, provided initial values of R_2 and R_3 are given at a known value of R_x. The energy equation, equation (13), is then soluble with the aid of equation (27), an initial value of η and an assumption for the magnitude of Δ. However, it is more convenient to measure flow properties at the slot, i.e. u_G, y_C and $\dot{m}''_C$, than to determine initial values of R_2, R_3 and η at some downstream location. Consequently, the present method was extended to provide initial condition correlations for R_2 and R_3; the initial value of η is readily obtained from equation (13) and the value of $R_{\theta,1}$, at the slot.

A value of downstream position, corresponding to a value of x/y_C of 10, was chosen as the R_x location at which initial values of R_2 and R_3 should be provided since at this point the potential core region has disappeared and the velocity profiles are generally well described by two parameters.

3.3.1 *The correlation for* $(R_2)_{x/y_C=10}$. In the absence of wall shear stress and pressure gradient, conservation of momentum implies that

$$(R_2)_{x/y_C=10} = R_{2,C} + R_{2,u} \qquad (28)$$

where

$$R_{2,C} = \frac{u_G}{\nu}\int_0^{y_C} \frac{u}{u_G}\left(1 - \frac{u}{u_G}\right)\mathrm{d}y \qquad (29)$$

$$R_{2,u} = \frac{u_G}{\nu}\int_{y_C}^\infty \frac{u}{u_G}\left(1 - \frac{u}{u_G}\right)\mathrm{d}y. \qquad (30)$$

Also, it may be shown that for a uniform velocity profile at the slot

$$R_{2,C} = R_C(1 - m) \qquad (31)$$

whereas for a parabolic profile

$$R_{2,C} = R_C(1 - \tfrac{6}{5}m). \qquad (32)$$

This shows that $R_{2,C}$ is relatively insensitive to the exact shape of the slot profile and may, with small error, be equated to $R_C(1 - m)$.

Thus

$$\frac{R_{2.10} - R_{2.u}}{R_C(1 - m)} = 1. \quad (33)$$

However, the assumptions of zero wall shear stress may be inappropriate and consequently an equation of the form*

$$\frac{R_{2.10} - R_{2.u}}{R_C(1 - m)} = f(m, R_C) \quad (34)$$

has been adopted, where the function $f(m, R_C)$ was determined from experimental data and found to be

$$f(m, R_C) = 0{\cdot}9 + 0{\cdot}2\,[1 - e^{-0{\cdot}3m}]. \quad (35)$$

Figure 6 indicates this relationship and the experimental data from which it was derived.

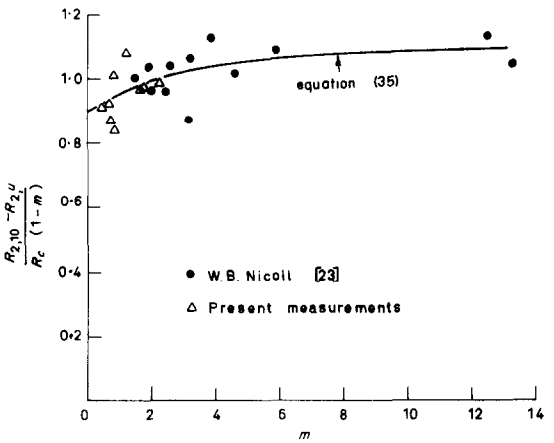

FIG. 6. The correlation equation for $R_{2.10}$.

Figure 7 indicates the derivations of the measured values of $R_{2,10}$ from those predicted with the aid of equations (34) and (35). It may be seen from these figures that the correlation equation predicts very well the data of Nicoll [23] and of the present measurements although the slot velocity profiles in these two cases were very different: the former was almost uniform and the latter was essentially parabolic.

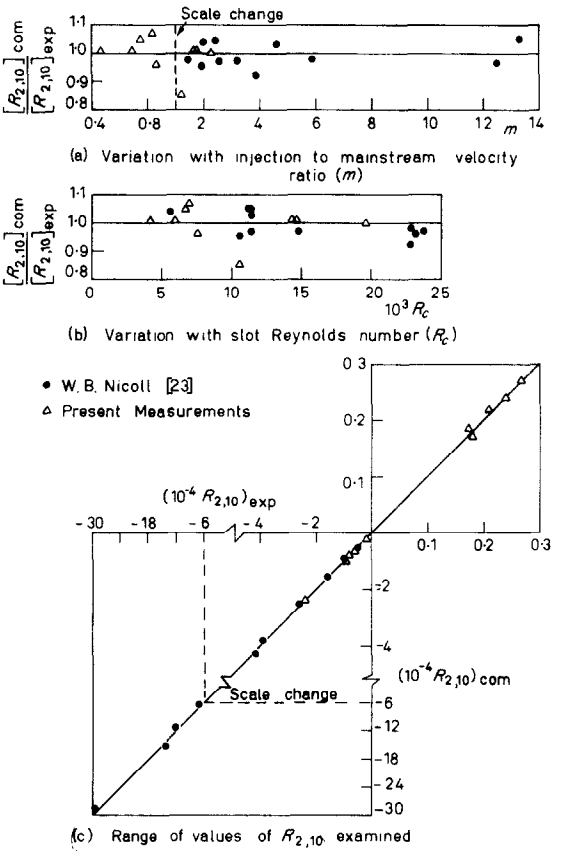

FIG. 7. Comparison between the experimental values of $R_{2,10}$ and those computed with the aid of equation (45).

3.3.2 *The correlation for* $(R_3)_{x/y_C=10}$. The method used in sub-section 3.3.1 was also used to obtain initial values for R_3 but the standard deviation of the resulting correlation equation proved to be somewhat greater than that obtained for the R_2 correlation. Consequently the following alternative approach was employed.

The flow downstream of the top lip of the injection slot spreads as a free shear layer.

* It should be noted that the function on the right-hand side of equation (34) could be extended to take account of pressure gradient. Unfortunately the authors are unaware of any suitable data.

Experiment shows that the width of a free shear layer, W, is approximately described by the equation

$$\frac{W}{x} = 0{\cdot}27\left|\frac{1-m}{1+m}\right|. \tag{36}$$

Thus, neglecting any inclination of the shear layer, the total boundary-layer thickness, y_G, is given by

$$y_G = y_c + \frac{W}{2} \tag{37}$$

so that

$$R_{G,10} = \frac{R_c}{m}\left\{1 + 1{\cdot}35\left|\frac{1-m}{1+m}\right|\right\}. \tag{38}$$

Since the constants 1 and 1·35 were obtained using crude assumptions, it is more appropriate to write

$$R_{G,10} = \frac{R_C}{m}\left\{a + b\left|\frac{1-m}{1+m}\right|\right\} \tag{39}$$

and to determine a and b from wall jet data, having first related $R_{G,10}$ to $R_{2,10}$ and $R_{3,10}$.

In order to relate $R_{G,10}$ to $R_{2,10}$ and $R_{3,10}$ it is necessary to make an assumption regarding the shape of the velocity profile. For simplicity, it is here assumed that this profile is linear. This assumption and the definitions of R_G, R_2 and ζ, as shown previously, leads to the equation

$$R_{G,10} = 6R_{2,10}/(1-\zeta_{10})(1+2\zeta_{10}) \tag{40}$$

which together with equation (39) gives

$$a + b\left|\frac{1-m}{1+m}\right| = \frac{-3mR_{2,10}}{R_C\left\{\left[\frac{2}{3}\frac{R_{3,10}}{R_{2,10}} - \frac{5}{4} + \sqrt{\left(\frac{2}{3}\frac{R_{3,10}}{R_{2,10}}\left[\frac{2}{3}\frac{R_{3,10}}{R_{2,10}} - 1\right]\right)}\right]^2 - \frac{9}{16}\right\}} = \frac{3mR_{2,10}}{R_C\left\{\frac{9}{16} - \left(\zeta_{10} - \frac{1}{4}\right)^2\right\}}. \tag{41}$$

Figure 8 indicates that suitable values for a and b are 1·3 and 1·24 respectively and Fig. 9 indicates the deviations of the measured values of $R_{3,10}$ from those predicted with the aid of equation (28) and the constants 1·3 and 1·24. Again it may be seen that the predicted values are very close to the measured ones.*

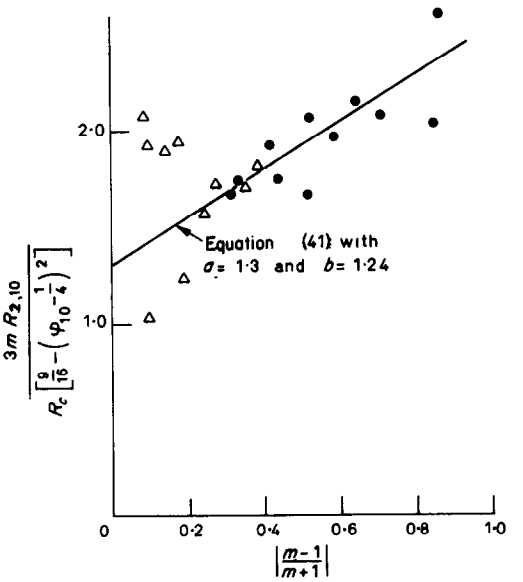

FIG. 8. The correlation equation for $R_{3,10}$.

3.3.3 *The initial value of effectiveness.* The integration of equation (13) implies that

$$(\eta R_{\theta,1}) = \text{constant} \tag{42}$$

and this constant is the φ flux at the slot divided by $(\varphi_C - \varphi_G)$ so that

$$(\eta R_{\theta,1}) = R_C. \tag{43}$$

With the aid of equation (27), equation (43) may

* The correlation equation for $R_{3,10}$, like that for $R_{2,10}$, is based on data for which the pressure gradient is nominally zero and for which $R_{2,u}$ is small.

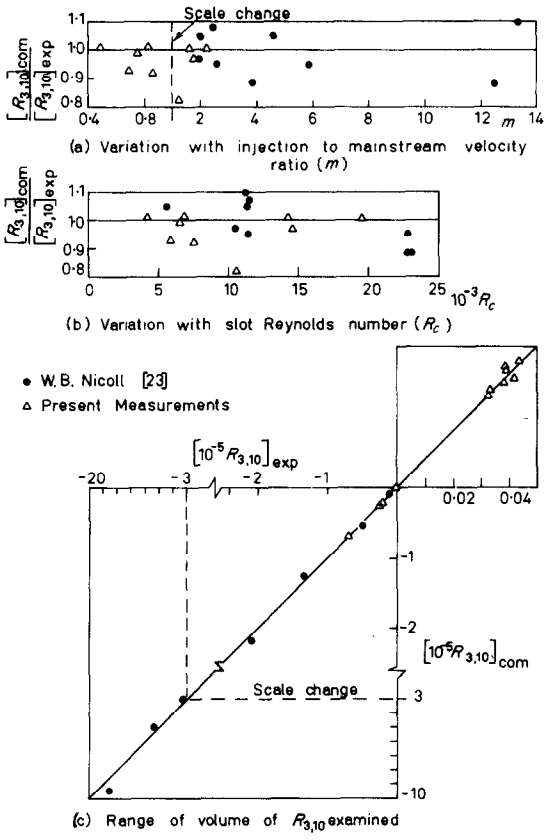

FIG. 9. Comparison between the experimental values of $R_{3,10}$ and those computed with the aid of equation (41) and the constants $a = 1{\cdot}3$, $b = 1{\cdot}24$.

be re-written as

$$\frac{\eta R_2}{(1-\zeta)(1+2\zeta)}\left[(\zeta-1)\left(3-\frac{1}{\Delta}\right)+3\Delta\right]=R_C \tag{44}$$

and thus an independent initial correlation for η is unnecessary.

4. COMPARISON BETWEEN MEASUREMENTS AND PREDICTIONS

Comparisons of the values of effectiveness predicted by the procedure described in Section 3 with the present measurements and with the measurements of Seban and Back [22] are shown in Fig. 10. These data were chosen for comparison because the boundary layers on the upper lip of the slot were, in general, relatively thin [i.e. $R_{2,u}$ much less than $R_C(1-m)$]; the exception being the present authors' runs 4 and 5. In all cases the initial conditions for the predictions were obtained from the initial condition correlations described in section 3.3, using the values of R_C and m reported by the appropriate author. For the present measurements, measured values of $R_{2,u}$ were used in the initial condition correlations; for the data of Seban and Back, $R_{2,u}$ was taken as zero, an assumption justified by the geometry of their experimental apparatus and by the large values of the flow parameter, m, associated with the data.

In general, the comparisons are satisfactory and require little comment. In the immediate vicinity of the slot, however, it should be noted that the predicted values are greater than unity; this is a direct consequence of the inaccuracy of the linear profile in this region but it is of little practical significance since the measured values of effectiveness in this region are close to unity.

Two predictions are shown for the present authors' run 4, the solid line being the prediction using the measured value of $R_{2,u}$ in the initial condition correlation, and the dashed line being the prediction based on the assumption that $R_{2,u}$ is zero. It may be observed that the prediction neglecting $R_{2,u}$ is better. This is a consequence of the inapplicability of the initial condition correlations when $R_{2,u}$ is appreciable compared to $R_C(1-m)$ in run 4 the respective values of these quantities were approximately 700 and -2680. This comparison does suggest that reasonable predictions of effectiveness may be obtained using the present method even in cases where the basic theoretical model is incorrect provided $R_{2,u}$ is neglected: this would of course only be true for zero pressure-gradient flows since only in this case is the predicted hydrodynamic, and hence thermal, development of the flow insensitive to the absolute value of R_2. (All the measurements discussed in this section have nominally zero pressure gradient.) To test the limitations of this hypothesis, the

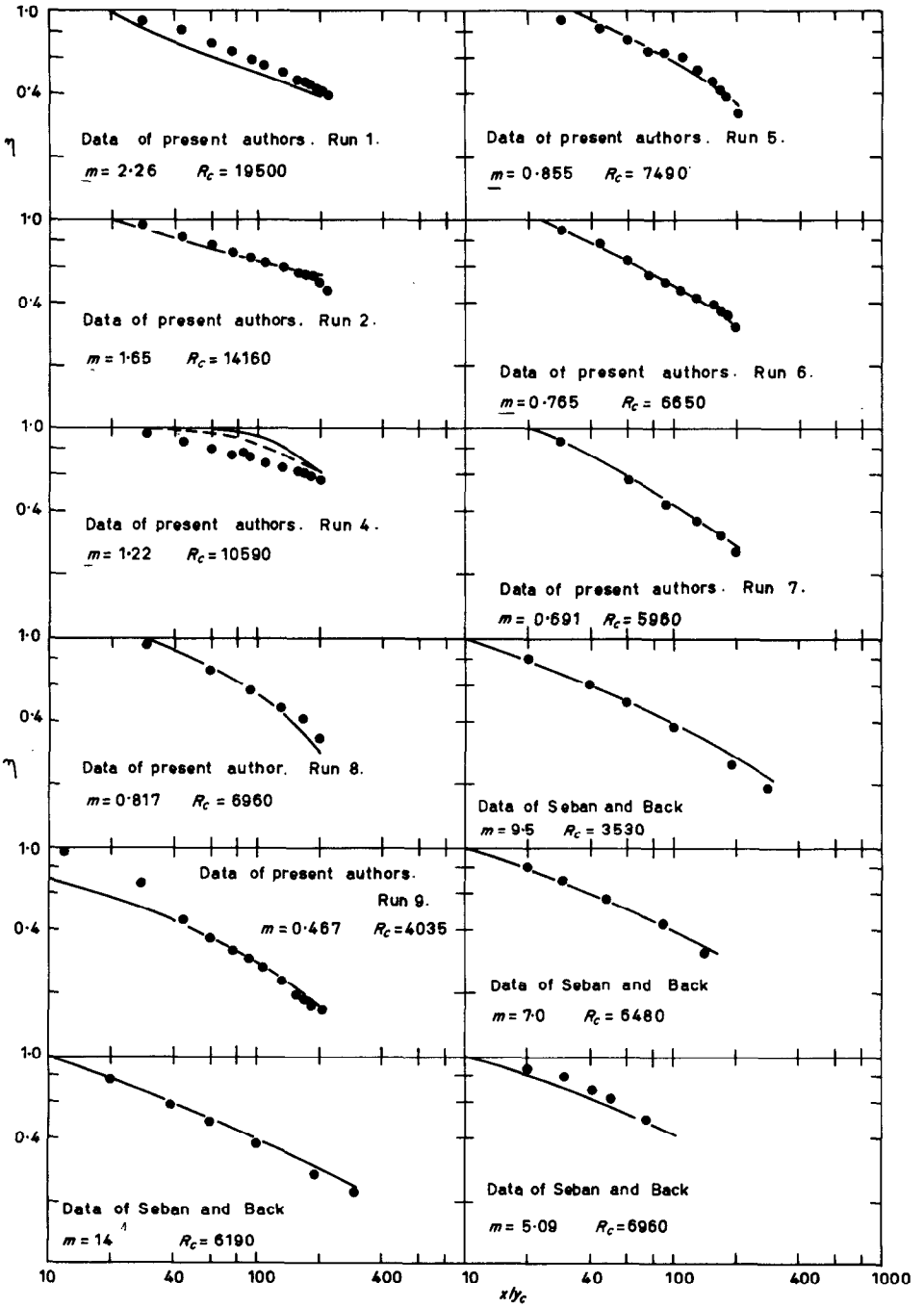

FIG. 10. Comparison of measured and predicted values of effectiveness: measurements of present authors and of Seban and Back [22].

present method was applied to the data of Chin *et al.* [3]. From the description of their experimental apparatus (the nominal origin of the boundary layer on the upper lip was reported to be 41·5 in upstream of the plane of the slot exit) it may be inferred that $R_{2,u}$ is large compared to $R_C(1-m)$. The resulting comparisons of prediction and measurement are shown in Fig. 11. This figure shows that despite the inapplicability of the initial condition correlations and the resultant large error in $R_{2,10}$ if $R_{2,u}$ is neglected, the predictions are reasonable for values of m not in the immediate vicinity of unity: when m is near unity the predicted values of effectiveness are too high.

5. DISCUSSION

The comparisons introduced in Section 4 indicate that the present method of prediction yields accurate values of the adiabatic wall effectiveness in those situations where the initial condition correlations and the auxiliary equation relating $R_{\theta,1}$ to hydrodynamic quantities can be expected to apply: namely, when the upstream boundary layer is small and at distances of, say, more than 10 slot heights downstream. Further, for zero pressure gradient flows, the predictions based on the neglect of the upstream boundary layer are reasonable except when m is near unity; when m is near unity the predictions are too high. In spite of these

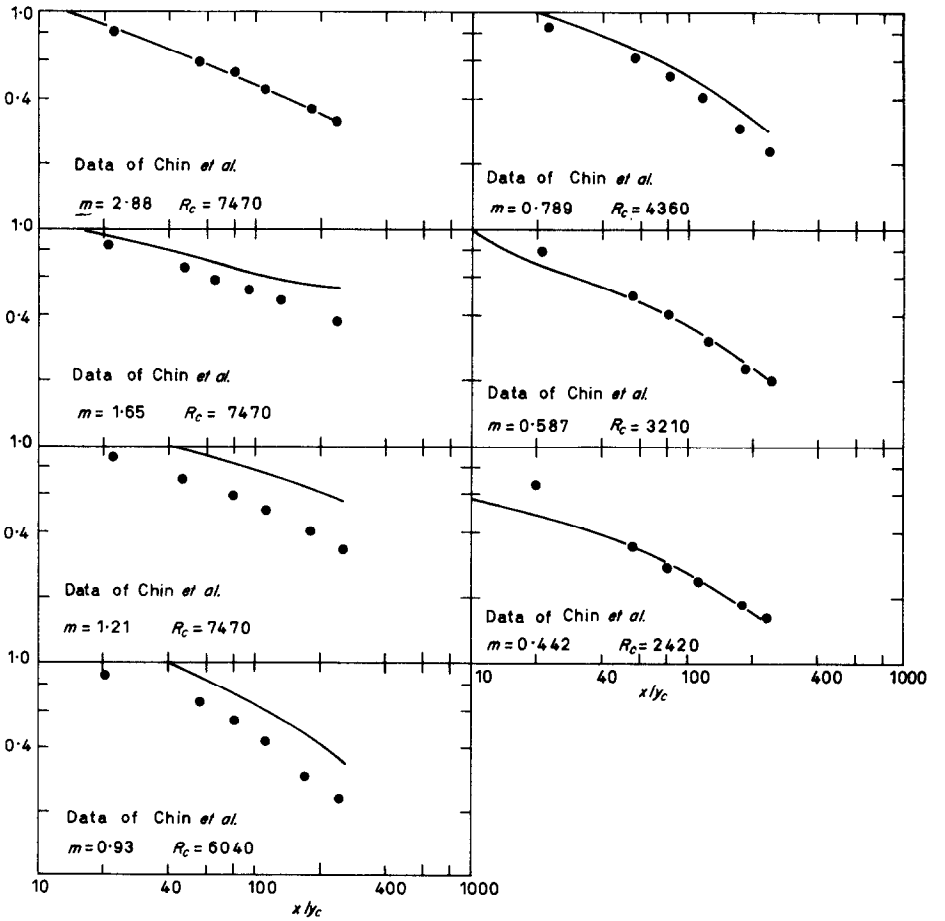

FIG. 11. Comparison of measured and predicted values of effectiveness: measurements of Chin *et al.* [3]. (Dimensions in inches.)

successes it must be remembered that the fundamental limitation of the present method to flows with thin upstream boundary layers is significant, particularly for non-zero pressure gradients. It is therefore appropriate co compare the present methods of predicting effectiveness with previous methods which do not suffer from this limitation.

To the present authors' knowledge, the only previous theory with sufficient flexibility to apply to the problem considered here, namely the prediction of adiabatic wall effectiveness for arbitrary pressure gradients, for values of m both greater than and less than unity, and for arbitrary upstream boundary layers, is the theory presented by Patankar and Spalding [17]. The theory presented by these authors is of the "parametric type" in which the dependent variables in the governing equations are parameters of the assumed families of velocity and φ profiles. This approach has the advantage of greater flexibility in that the number of parameters can be arbitrarily increased to deal with more complex flow situations: specifically it is easy to include as a variable, the ratio of the thermal to hydrodynamic boundary-layer thickness and hence to escape this limitation. The disadvantages of the method described in reference [17] are of three types. First the dependent variables are ill-defined experimentally and it is not always possible to obtain from experimental quantities the required initial conditions. Secondly, when predictions do not correspond to measurement, it is difficult to determine which assumption should be modified: in the present explicit approach the auxiliary equations can be modified individually to correspond to the experimental facts. Thirdly, the numerical procedure involved in obtaining a prediction, involves the iterative solution of implicit equations, thereby greatly increasing the computational effort involved. This last disadvantage is of little importance when large automatic computers are available, but it is of considerable importance to the practising engineer who is without this facility.

The method described in reference [16] also suffers from the three disadvantages listed above. In addition it is not suitable for cases where the upstream boundary layer is large because, as in the present method, the coextensiveness of the thermal and hydrodynamic boundary layers is assumed.

6. CONCLUSIONS

(i) The present method of prediction yields accurate results for both adiabatic wall and impervious wall effectiveness provided the upstream boundary layer is thin.

(ii) The initial condition correlations presented allow the predictions of effectiveness to be based on the flow parameters at the slot over which the designer has direct control, namely m and R_C.

(iii) The successful prediction of measurements of impervious wall effectiveness and adiabatic wall effectiveness suggests that the total Lewis number, for small mass concentrations of helium in air, may be taken as unity.

ACKNOWLEDGEMENTS

The authors gratefully acknowledge the continuing support and encouragement of Professor D. B. Spalding and wish to thank Mr. M. P. Escudier for the use of various computer programs.

The financial support of the Ministry of Aviation (Contract numbers PD/37/027 and PD/37/043 is gratefully acknowledged.

REFERENCES

1. K. Wieghardt, Hot air discharge for de-icing, A.A.F. Translation No. F-TS-919-RE (1946).
2. R. A. Seban, H. W. Chan and S. Scesa, Heat transfer to a turbulent boundary layer downstream of an injection slot, A.S.M.E. Paper No. 57-A-36 (1957).
3. J. H. Chin, S. C. Skirvin, L. E. Hayes and A. Silver, Adiabatic wall temperature downstream of a single injection slot, A.S.M.E. Paper No. 58-A-107 (1958).
4. S. S. Papell and A. M. Trout, Experimental investigation of air film cooling applied to an adiabatic wall by means of an axially discharging slot, NASA TN D-9 (August 1959).
5. S. S. Papell, Effect on gaseous film cooling of injection through angled slots and normal holes. NASA TN D-299, 1960.

6. R. A. SEBAN, Heat transfer and effectiveness for a turbulent boundary layer with tangential fluid injection, *J. Heat Transfer* **82 C**, 303 (1960).
7. J. H. CHIN, L. E. HAYES, S. C. SKIRVIN and F. BURGGRAF, Film cooling with multiple slots and louvers, *J. Heat Transfer* **83 C**, 281 (1961).
8. J. P. HARTNETT, R. C. BIRKEBAK and E. R. G. ECKERT, Velocity distributions, temperature distributions, effectiveness and heat transfer for air injected through a tangential slot into a turbulent boundary layer, *J. Heat Transfer* **83 C**, 293 (1961).
9. G. H. HALLS, Some problems associated with cooling gas turbine combustion chambers, Rolls Royce Ltd., Aero Engine Division, Reference TB/GAH 1/MB (1963).
10. A. E. SAMUEL and P. N. JOUBERT, Film cooling of an adiabatic flat plate in zero pressure gradient in the presence of a hot mainstream and cold tangential secondary injection, A.S.M.E. Paper No. 64-WA/HT-48 (1964).
11. E. R. G. ECKERT and R. C. BIRKEBACK, The effects of slot geometry on film cooling, in *Heat Transfer and Thermodynamics Education*, edited by H. A. JOHNSON, pp. 150–163. McGraw-Hill, New York (1964).
12. R. B. PRICE, Summary of cooling tests carried out on a film-cooled parallel duct, Bristol Siddeley Engines Ltd., Advanced Propulsion Research Grants, Report No. A.P. 5312 (May 1965).
13. J. H. WHITELAW, The effect of the geometry of the injection region on wall cooling processes, Aero. Res. Council Report, A.R.C. 27373 (1965).
14. D. B. SPALDING, V. K. JAIN and W. B. NICOLL, Film cooling in incompressible turbulent flow: examination of experimental data for the adiabatic wall temperature, Aero. Res. Council Report A.R.C. 25311 (November 1963).
15. D. B. SPALDING, The prediction of adiabatic wall temperatures in film cooling systems, *AIAA Jl* **3**, 965–967 (1965).
16. D. B. SPALDING, A unified theory of friction, heat transfer and mass transfer in the turbulent boundary layer and wall jet, Aero. Res. Council Report, A.R.C. 25925 (1964).
17. S. V. PATANKAR and D. B. SPALDING, A calculation procedure for heat transfer by forced convection through two-dimensional uniform-property turbulent boundary layers on smooth impermeable walls, Aero. Res. Council Report, A.R.C. 27432 (1965).
18. M. P. ESCUDIER, W. B. NICOLL, D. B. SPALDING and J. H. WHITELAW, The decay of a velocity maximum in a turbulent boundary layer, Dept. Mech. Engng, Imperial College, Report TWF/TN/13 (May 1966). (Accepted for publication by *Aero. Quart.*)
19. J. H. WHITELAW, An experimental investigation of the two-dimensional wall jet, Aero. Res. Council Report, A.R.C. 28179 (1966).
20. M. P. ESCUDIER and W. B. NICOLL, The entrainment function in turbulent boundary layer and wall jet calculations, *J. Fluid Mech.* **25**, 337–366 (1966).
21. M. P. ESCUDIER, W. B. NICOLL and D. B. SPALDING, An explicit drag law for uniform density turbulent boundary layers, Dept. Mech. Engng, Imperial College, Report TWF/TN/12 (June 1966).
22. R. A. SEBAN and L. H. BACK, Velocity and temperature profiles in a wall jet, *Int. J. Heat Mass Transfer* **3**, 255–265 (1961).
23. W. B. NICOLL: Unpublished data relating to the experiments reported in reference [20].

Résumé—L'article présente de nouvelles mesures de l'efficacité d'un pariétal bi-dimensionnel et un processus de calcul que l'on montre prévoir d'une façon précise les valeurs mesurées pour une classe restreinte, mais d'importance pratique, de conditions d'injection.

Les mesures ont été effectuées dans la gamme du rapport de la vitesse massique dans la fente à l'écoulement libre allant de 0,467 à 2,26, en utilisant l'hélium comme un gaz traceur et un équipement de chromatographie gazeuse pour détecter les concentrations.

La méthode de prévision emploie des relations empiriques pour rattacher les propriétés d'écoulement dans la fente à celles en aval du noyau potentiel.

A partir de là, on emploie une méthode explicite de résolution des équations de la couche limite. Les avantages et les désavantages de la méthode sont discutés.

Zusammenfassung—Die Arbeit behandelt neue Messungen über die Wirksamkeit zweidimensionaler Wanddüsen und ein Rechenverfahren, das mit guter Genauigkeit erlaubt die gemessenen Werte für eine begrenzte, aber praktisch wichtige Reihe von Einblasbedingungen zu berechnen.

Die Messungen wurden durchgeführt für Verhältnisse von Schlitz- zu Freistromgeschwindigkeit von 0,467 bis 2,26, unter Benützung von Helium als Spürgas und einer gaschromatischen Einrichtung zur Feststellung von Konzentrationen.

Die Rechenmethode stützt sich auf empirische Korrelationen, um die Strömungseigenschaften am Schlitz mit jenen stromabwärts vom Potentialkern zu verbinden. Danach wird eine ausführliche Lösungsmethode für Grenzschichtgleichungen angewandt. Die Vorund Nachteile der Methode werden diskutiert.

Аннотация—В статье приводятся новые данные по измерениям эффективности пристенной струи, а также описывается метод расчета, дающий результаты, близкие к измеренным величинам для ограниченного, но практически важного класса условий вдува.

Измерения проводились в диапазоне отношений массовой скорости на выходе из щели к этой величине в свободном потоке от 0,467 до 2,26. В качестве индикаторного газа использовался гелий, концентрация которого измерялась методом газовой хроматографии.

Метод расчета использует эмпирические соотношения, связывающие характеристики течения в щели с характеристиками течения в потенциальном ядре. Отмечаются преимущества и недостатки метода.